inorganics

MDPI

Article

Cost Optimization of Graphene Oxide-Modified Ultra-High-Performance Concrete Based on Machine Learning Methods

Hui Lv [1], Mingfeng Du [2], Zijian Li [2], Li Xiao [1] and Shuai Zhou [2,*]

[1] China Merchants Chongqing Communications Technology Research and Design Institute Co., Ltd., Chongqing 400067, China
[2] College of Materials Science and Engineering, Chongqing University, Chongqing 400045, China
* Correspondence: shuaizhou@cqu.edu.cn

Abstract: The use of carbon nanomaterials in ultra-high-performance concrete (UHPC) to improve its mechanical properties and durability is growing. Graphene oxide (GO) has emerged as one of the most promising nanomaterials in recent years for enhancing the properties of UHPC. The majority of research so far has been on the properties of UHPC enhanced with GO, but its high cost has limited its application in engineering. This work suggests a machine learning (ML)-based approach to optimize the mix ratio in order to lower the cost of graphene oxide-modified UHPC. To do this, an artificial neural network (ANN) is used to create the prediction model for the 28-day compressive strength and slump flow of UHPC. The performance of this model is then compared using nine different ML techniques. Subsequently, considering the restrictions of the UHPC component content, component proportion, and absolute volume, a genetic algorithm (GA) is adopted to lower the UHPC cost. The sensitivity analysis is carried out in the end. This study's findings indicate that there is a decent degree of prediction accuracy since the difference between the ANN model's predictions and the experimental outcomes is just 10%. The cost of UHPC optimized by GA is reduced to 776 $/m^3, significantly lower than the average cost of UHPC.

Keywords: ultra-high-performance concrete (UHPC); graphene oxide (GO); machine learning; cost

Citation: Lv, H.; Du, M.; Li, Z.; Xiao, L.; Zhou, S. Cost Optimization of Graphene Oxide-Modified Ultra-High-Performance Concrete Based on Machine Learning Methods. *Inorganics* **2024**, *12*, 181. https://doi.org/10.3390/inorganics12070181

Academic Editors: Ben McLean and Alister Page

Received: 30 May 2024
Revised: 19 June 2024
Accepted: 21 June 2024
Published: 28 June 2024

1. Introduction

Ultra-high-performance concrete (UHPC) is a popular cement-based material. It can achieve very high strength and toughness by optimizing its material composition. UHPC has been used in many structures around the world [1,2]. Due to the rapid development of carbon nanomaterials in recent years and the need to further improve the performance of UHPC, many scholars have begun to use carbon nanomaterials as additives for UHPC [3]. Carbon nanomaterials suitable for cement-based materials include carbon nanotubes [4,5], graphene sulfonate nanosheets [6], and graphene oxide (GO) [7]. They have been proven to reduce the amount of cement used in UHPC without affecting performance and produce a new generation of multifunctional cement-based materials. As a nanomaterial with a unique two-dimensional structure, GO can improve the overall performance of UHPC at very low contents, including enhancing compressive strength, tensile strength, and flexural strength, as well as reducing permeability and improving durability [8]. Compared with other carbon-based nanomaterials, such as graphene nanosheets or carbon nanotubes, GO is easily dispersed in water [9]. Graphene oxide-based materials and applications are currently of great interest due to their unique qualities that can substantially improve the properties of composite materials. Graphite oxide is created when graphite undergoes oxidation. Graphene oxide is then formed ($C_{54}H_{17}$ + O + $(OH)_3$ + COOH). The chemical process that creates graphite oxide from concentrated acids and a strong oxidizing agent is commonly used to create exfoliated graphite. GO sheets feature a high degree of hydrophilicity due to the functionalization of carboxyl and carbonyl groups at the edges and hydroxyl and

epoxide groups at the basal planes. According to the study by Chu et al. [10], the optimal dosage of GO is 0.05% of the cementitious material, which can improve the compressive and flexural strength of UHPC. Wu et al. [8] found that the compressive strength and flexural strength of UHPC increased with the addition of GO and proposed the optimal dosage of 0.02% by weight of the cement. Luo et al. [11] found that 0.02% GO significantly increased the flexural strength of UHPC and effectively strengthened the interface between the steel fibers and matrix. Carbon atoms with sp2- and sp3-hybridized orbitals make up GO, a hexagonal network. Hydroxyl and epoxide groups make up a large number of the functional groups in the GO structure. Because of the hydrophilic quality that these functional groups confer, graphene oxide is readily dissolved in water. Making use of GO's strong water dispersion capability makes it possible to blend components based on cement. GO also possesses a great specific area, extremely high strength, and remarkable flexibility, all of which may be used to adjust the cement matrix qualities in an efficient manner. The durability, mechanical characteristics, and microstructures of concrete are all directly correlated. GO has the capacity to improve the cement matrix's pore structure, increasing the concrete's ability to withstand chemical assaults and fluid infiltration. This may significantly slow down the corrosion process of steel reinforcement. Hence, GO has a positive impact on the advancement of UHPC.

At present, the development of UHPC still relies on time-consuming and laborious trial-and-error methods. In addition to the complexity of raw materials, its high cost is also the main reason limiting the widespread application of UHPC containing GO. With the advancement of nanotechnology, the industrial-grade GO can be produced at lower manufacturing costs. Therefore, using GO to improve the performance of cement-based materials is economically feasible. Currently, most research has focused on enhancing the macro and micro performances of UHPC with GO, and further research is needed to use GO from an economic perspective.

With the rapid development of artificial intelligence, machine learning (ML) algorithms are gradually being applied to material performance evaluation and optimization [12–15]. Many types of cement-based materials have been optimized using ML methods, like graphene-modified cementitious composites [16,17], rubber-modified recycled aggregate concrete [18], reinforced concrete [19], sustainable high-strength concrete [20], and waste glass reinforced cement [21]. ML is a branch of artificial intelligence that can automatically extract hidden relationships from high-dimensional data and transform them into explicit information or knowledge. ML provides an opportunity to capture the complex multidimensional relationships between the input (mix ratio) and output (material properties) while reducing the need for trial-and-error methods in specific designs. It uses historical data to train models, which can later be used to predict material properties. This method has been used to predict the properties of concrete, demonstrating its ability and versatility. Farooq et al. [22] introduced four machine learning algorithms, namely random forest, gene expression programming, artificial neural networks (ANN), and decision trees, to predict the performance of concrete. Shamiri et al. [23] developed a new ML model for predicting the strength of UHPC, which has high accuracy and good generalization ability. In addition to predicting material properties, the ML methods have also demonstrated excellent capabilities in cost optimization. Lee et al. [24] optimized the cost of UHPC using neural networks and harmonic search algorithms. Cheng et al. [25] used support vector regression and a genetic algorithm (GA) to optimize the mix proportion of UHPC, achieving the minimum cost. Through the literature review, it can be noted that using ML methods in UHPC performance prediction and cost estimation has the following advantages such as solving nonlinear problems, identifying large amounts of material data, confirming valid data, and correcting corresponding relationships to better simulate future data. Here, ML methods are adopted to design GO-modified UHPC. Using ML methods to roughly estimate and optimize the performance of concrete will greatly save time and costs in testing and producing specimens.

Figure 1 shows the flowchart of the whole framework of this research, which can be categorized into two stages: the first one is the prediction model construction and the other one is the establishment of the cost-optimization model. This research first establishes a prediction model for the 28-day compressive strength and slump flow of UHPC using ANN. The prediction performance of nine distinct ML methods is compared. Taking the 28-day compressive strength, slump flow, component content, component proportion, and absolute volume as constraints, the UHPC mix ratio with the lowest cost is obtained through GA optimization. Finally, sensitivity analysis is conducted to evaluate the importance of each raw material in UHPC on its performance. The purpose of this research is to explore the effect of GO on the properties of UHPC and obtain the lowest cost ratio through ML under the condition of meeting the engineering requirements for concrete performance, thereby promoting the application of GO-modified UHPC.

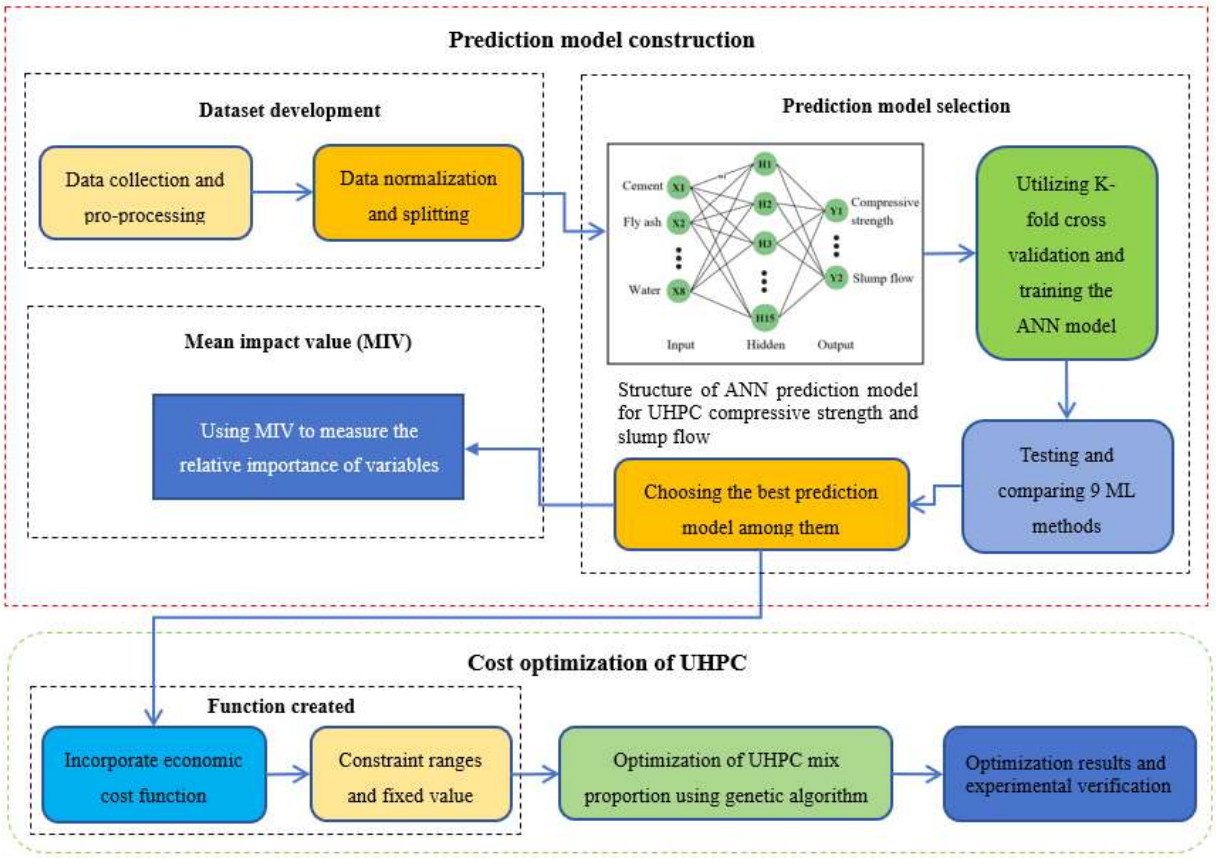

Figure 1. Flowchart of the entire framework.

2. Modeling Methods

2.1. Artificial Neural Network

ANN is an information processing system composed of interconnected processing units similar to neurons, which abstracts, simplifies, and simulates the organizational structure and operational mechanism of the animal brain. ANN simulates complex nonlinear relationships between inputs and outputs through multiple levels of neural nodes and weight connections. In addition to containing input and output layers, there are also one or more hidden layers. ANN usually has good generalization ability. By adjusting the network structure and parameters, they can adapt to various types of data and problems and can make more accurate predictions on unseen data. The input layer contains nodes with an equal number of features, each representing a feature of the input data, having multiple hidden layers to capture complex relationships in input data. Each hidden layer contains multiple neuron nodes, and each neuron learns to adjust to the appropriate weights to

extract features and generate appropriate outputs. By introducing nonlinear activation functions, such as ReLU or Sigmoid functions, into hidden layer neurons, they enhance the fitting ability of nonlinear systems. For regression tasks, the output layer uses one or more nodes to represent the output variables of the regression problem. ANN adapts to input data by setting appropriate weights and biases. ANN often adopts the error backpropagation algorithm to systematically solve the problem of learning hidden layer connection weights in multi-layer neural networks [26]. The basic principle of ANN is displayed in Figure 2.

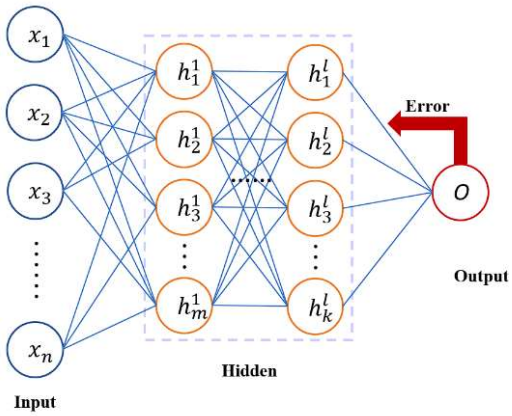

Figure 2. The basic structure of ANN.

2.2. Genetic Algorithm

GA was first proposed by John Holland in the United States in the 1970s and later summarized by DeJong, Goldberg, and others to form a class of simulated evolutionary algorithms [27]. In order to acquire the best answers, a computational model mimics Darwin's theory of biological evolution's genetic and natural selection processes. Initialization, individual assessment, selection operation, cross operation, mutation operation, and termination condition judgment are the six parts that make up the fundamental workings of GA. Fitness is a term used in evolutionary theory to describe an individual's capacity for environmental adaptation. The fitness function is employed in GA as the evaluation function to determine the individual quality within a population. In this study, different mix ratios of UHPC are used as different individuals in the population. The fitness function is the UHPC cost function. The mix ratio of GO-modified UHPC with the lowest cost is the individual with the greatest fitness, achieved after selection, crossover, and mutation procedures. For further information on the particulars of GA, see earlier research [28].

2.3. K-Fold Cross-Validation

K-fold cross-validation (CV) was developed by Stone in 1974 and widely used in ML to select the appropriate hyperparameters [29]. K-fold CV is a commonly used model evaluation method. In K-fold CV, the original dataset is divided into k equal subsets, one of which is retained as the validation set, while the other k-1 subsets are used to train the model. This process is repeated k times, and each subset is used as a validation set. The final result is the average of k's validation results. This method fully utilizes all data for training and validation; reusing these subsets to train and validate the model can reduce bias and variance issues caused by improper dataset partitioning and provide a more accurate estimate of the model's generalization ability. Due to each sample being used as a validation set, the model will not overly rely on specific training validation segmentation, thereby reducing the risk of overfitting. The main process of the K-fold CV is displayed in Figure 3.

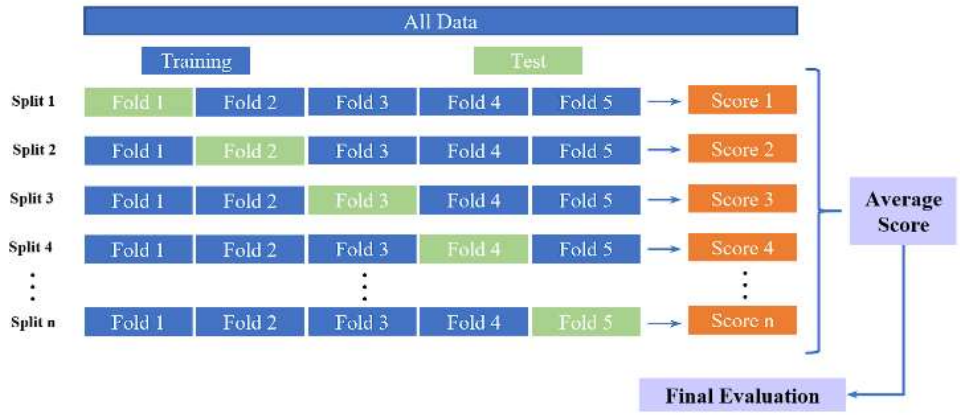

Figure 3. The theory of K-fold CV.

For this investigation, $k = 10$ is chosen. The study uses the correlation coefficient (R) and mean squared error (MSE) to assess how well the hyperparameters work. The difference between the experimental and predicted results is measured by the MSE. The model adopts R to determine the degree of correlation between variables. Equations (1) and (2) are used to compute the MSE and R.

$$MSE = \frac{1}{n}\sum_{i=1}^{n}(y_{mi} - y_i)^2 \quad (1)$$

$$R = \frac{\sum_{i=1}^{n}(y_{mi} - \overline{y_{mi}})(y_i - \overline{y})}{\sqrt{\sum_{i=1}^{n}(y_{mi} - \overline{y_{mi}})^2}\sqrt{\sum_{i=1}^{n}(y_i - \overline{y})^2}} \quad (2)$$

where n is the number of samples; y_{mi} means the predicted result; and y_i refers to the experimental result.

2.4. Mean Impact Value

Mean impact value (MIV) is proposed to measure the relative importance of the variables that affect outcomes and is used to evaluate the features in ML methods. The specific operation process of MIV is as follows. Firstly, the ML model is trained through the original training sample P. After the model training is completed, each independent variable data in the original sample P is added or subtracted by 10% to form two new training samples, P_1 and P_2. Then, input the new samples P_1 and P_2 into the trained ML model to obtain two simulation results, Q_1 and Q_2. The difference between Q_1 and Q_2 is called the impact value (IV), and then IV is divided by the sample size to obtain MIV. This value can be used to determine the impact of input nodes on output nodes in the ANN model. Calculate the MIV value of each input node through the above operation process, whose absolute value reflects the correlation, and its plus–minus sign reflects the direction of the correlation. Sorting the MIV by their absolute values yields a relative ranking of the impact of each input node on the output value of the ANN.

3. Raw Materials and Experiments

3.1. Raw Materials

In the research, raw materials in UHPC include cement, fly ash, GO, silica fume, fine aggregate, steel fibers, superplasticizer, and water. Except for GO, the study considers the most basic raw materials, as it is not advisable to use too many different types of raw materials in the plant for producing UHPC. Portland cement is provided by Sichuan Esheng Company (Leshan, China). The fly ash adopts first-class fly ash with a specific surface area of 415 m^2/kg, provided by Chongqing Fuhuang Company (Chongqing, China). The silica fume is supplied by Shanghai Shanying Environmental Protection Technology Co., Ltd. (Shanghai, China). Table 1 summarizes the chemical composition and density of cement, fly ash, and silica fume. Machine-made sand has an apparent density of 2630 kg/m^3 and a

fineness modulus of 3.34, which is used as a fine aggregate. The polycarboxylic acid water-reducing agent, which has a 40% solid content and a 45% water-reducing rate, is made by China Construction West Construction Co., Ltd. (Chengdu, China), and was utilized in this experiment. The steel fiber's dimensions are 12 mm in length, 0.25 mm in diameter, and 1800 MPa for the ultimate tensile strength. The steel fibers are straight with a smooth surface. Its properties meet the requirements of GB/T31387–2015 [30]. GO is sourced from Jiazhaoye (Guangdong, China) New Materials Co., Ltd. Its technical parameters are listed in Table 2. There are many different types of GO. Chemical functionalization is one technique to rid the impact GO has on cement's flowability. Chemically functionalized graphene oxide may improve the fluidity of cement, while GO reduces the rheological properties of cement [31]. This research only investigates graphene oxide. Chemical-functionalized graphene oxide will be further considered in future research.

Table 1. Chemical compositions and densities of cementitious materials.

Composition	SiO_2 (%)	Al_2O_3 (%)	CaO (%)	MgO (%)	Na_2O (%)	K_2O (%)	Fe_2O_3 (%)	TiO_2 (%)	SO_3 (%)	P_2O_5 (%)	Density (kg/m^3)
Cement	21.39	5.15	61.04	2.82	0.64	0.62	3.86	0.85	3.1	0.10	3190
Fly ash	48.54	27.12	3.19				11.08		1.63		2270
Silica fume	94.57	0.67	0.34	0.23		0.82	0.15		2.07	0.90	2310

Table 2. Technical parameters of GO.

Thickness (nm)	Diameter (um)	Peelable (%)	Carbon (wt%)	Oxygen (wt%)	Sulfur (wt%)	Ash Content (wt%)	Tap Density (g/L)	Granularity
2	10.4	96	46.9	55.8	<3.6	<2.8	600	<85

3.2. The Preparation and Testing of UHPC

A total of 31 mix proportions were prepared for this experiment, of which 30 were used to confirm the ANN prediction model's accuracy in predicting UHPC's compressive strength and slump flow. The other mix ratio was designed for the validation of the GA optimization of UHPC. The mix ratio must accommodate the widest practical range. The goal of adding more samples was to broaden their coverage range, which will enhance the model's accuracy and prediction range.

Table 3 lists the mix ratios of each group of UHPC samples in the experiment. For sample preparation, please refer to the methods mentioned in the previous references [32,33]. The mixing program consists of four steps as follows: (1) Pre-mix the drinking water and GO in a separate container. Add a high-efficiency water-reducing agent and disperse the GO suspension using ultrasound to ensure uniform dispersion of GO in the water. (2) Mix the cement, silica fume, fly ash, and fine aggregates in a mixer for 2 min. (3) Add the pre-mixed solution and stir for two minutes. (4) Add steel fibers and mix the mixture for 5 min. Pour the fresh UHPC mixture into a pre-lubricated mold. Compact the cube sample on a vibration table. Afterwards, cover the sample with polyethylene sheets and cure it in the laboratory for 24 h. After demolding, cure the sample in a standard environment. The sample shall be cured for 28 days at a relative humidity greater than 95% and a temperature of $21 \pm 2\ ^{\circ}C$ until the time of testing. GO is prone to cluster in cement-based materials. Even when graphene oxide is modified by a superplasticizer before contact with cement paste, the graphene oxide in the paste remains partly agglomerated [32]. Therefore, ultrasound was used here for the dispersion of GO. The experiments have proved that ultrasound can uniformly disperse graphene oxide in cement-based materials [32–36].

Table 3. The mix ratios of UHPC in the experiments.

Cement (kg)	FA (kg)	GO (kg)	SF (kg)	Fine Aggregates (kg)	Steel Fibers (vol.%)	Superplasticizer (wt%)	Water (kg)
632	0	0.063	158	1316	2.0	1.8	223
642	0	0.128	148	1185	2.0	1.8	158
653	201	0.196	151	1008	2.0	1.8	161
675	125	0.270	115	1179	0.0	2.0	180
690	212	0.345	159	1061	3.0	1.8	191
692	0	0.415	148	1185	2.0	1.8	158
703	151	0.070	151	1005	2.0	1.8	161
718	0	0.144	127	1352	2.0	1.8	152
736	0	0.221	156	1182	2.0	1.8	173
741	198	0.296	148	1185	2.0	1.8	158
750	125	0.375	115	1104	0.0	2.0	180
763	191	0.458	106	1079	2.0	1.8	173
776	48	0.078	145	1212	2.0	1.8	165
777	0	0.155	108	1079	2.0	1.8	173
800	176	0.240	150	650	2.0	1.8	165
808	0	0.323	143	1189	2.0	2.0	175
811	0	0.406	143	1192	2.0	1.8	191
817	0	0.490	144	1202	2.0	1.8	180
840	0	0.084	148	1185	2.0	1.8	158
847	0	0.169	150	997	1.0	1.8	179
850	176	0.255	150	650	2.0	1.8	165
857	0	0.343	151	1008	1.0	1.8	191
861	0	0.431	152	1125	2.0	1.8	202
868	0	0.521	153	1021	3.0	2.0	183
870	0	0.087	154	1024	3.0	2.0	189
875	0	0.175	154	1144	2.0	1.8	206
890	0	0.267	157	1047	3.0	1.8	209
900	0	0.360	100	1350	0.4	2.5	170
903	0	0.452	159	1062	2.0	1.8	204
1000	0	0.600	0	1350	0.4	2.5	170

The fluidity of the fresh UHPC mixture was assessed by measuring its slump flow in accordance with Chinese Standard GB/T2419–2005 [37]. The compressive strength of the specimens was measured at 28 days. The specimens are 100 mm × 100 mm × 100 mm and were tested according to Chinese Standard GB/T 31387–2015 [30]. The main process of the experiment is illustrated in Figure 4.

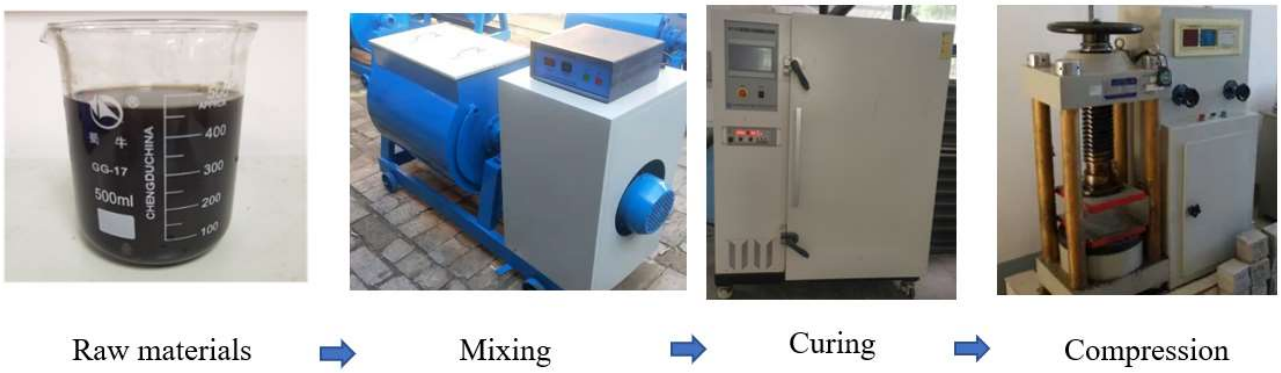

Figure 4. Flowchart of the experiments.

4. Modeling Based on Machine Learning

4.1. Set Up the Database

4.1.1. Data Sources

At first, a UHPC database was developed. The dataset of this study includes eight input parameters: cement content, fly ash content, GO content, silica fume content, fine aggregate content, steel fiber volume content, superplasticizer content, and water content in 1 m^3 UHPC. The two output parameters were the 28 d compressive strength and slump flow of UHPC. The 422 sets of experimental data for UHPC in this study come from existing literature [8,12,14,33,38–54], while 31 sets are from their own experimental data, with a total of 453 sets of data gathered. According to previous research [55], 453 sets of UHPC samples with different mix ratios are sufficient to develop ML models to predict their properties. We split the dataset into two groups, using thirty percent for testing and seventy percent for training. The ANN model was trained on the data from the training group and tested on the data from the testing group. The experimental data in the study served as the testing set to evaluate the ML model's ability to predict outcomes when combined with additional experimental results from the literature.

4.1.2. Data Normalization Processing

The original data must be normalized before training the ANN model, as variations in the input parameters might impact how well the model is trained. Described in another way, normalize the data within the interval [−1,1]. In addition to hastening the ANN model's convergence, data normalization processing can increase the model's prediction accuracy. The dataset in this study was normalized using the min–max normalization approach. In essence, min–max normalization applies linear modifications to a dataset by

$$X^* = (X - X_{min})/(X_{max} - X_{min}) \quad (3)$$

where X^* is the normalized data, X_{min} denotes the minimum value in the original dataset, and X_{max} means the maximum value in the original dataset.

4.2. The Prediction Model

4.2.1. Determination of ANN Model Structure

The relationship between the costs and raw materials was initially established using ANN. Next, the GA was utilized to improve the properties and cut expenses based on the pre-trained ANN model. ANN was used in this work to develop a UHPC performance prediction model. Cement, fly ash, GO, silica fume, fine aggregate, steel fiber, superplasticizer, and water made up the eight neurons in the input layer, designated X1 through X8 in that order. The neurons in the output layer are Y1 and Y2, which represent the UHPC's 28 d compressive strength and slump flow. Using a trial-and-error approach, the hyperparameter of the number of hidden layer neurons was determined.

The quantity of the ANN's hidden layer neurons influences the model's prediction accuracy. The prediction accuracy of the model was assessed in this study using the indicator *R* and *MSE*, and network training was completed on hidden layer nodes that ranged from five to twenty. Ten parts were randomly selected from the training set using a 10-fold CV, with one part serving as the verification set and the other nine as the training set. Each time, the procedure was carried out using distinct samples for the validation group. After applying 10-fold CV, the prediction was evaluated by averaging the error. Then, for comparison, the mean values of the *MSE* and *R* were investigated.

When the number of hidden layer neurons equals 16, the correlation coefficient *R* reaches its maximum. This value is closer to 1 than it is in other networks. When there are 16 hidden layer neurons, *MSE* also achieves its smallest value. As a result, the greatest correlation and least amount of error between the predicted and experimental values were found in the ANN model with 16 hidden layer neurons. To create the prediction model, an ANN network with 16 hidden layer neurons was used, as shown in Figure 5.

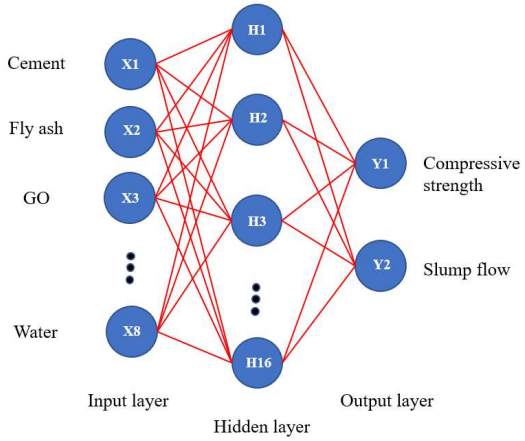

Figure 5. Structure of ANN prediction model for UHPC's compressive strength and slump flow.

4.2.2. Training of ANN Model

To create a prediction model for UHPC's 28-day compressive strength and workability, the data are trained several times after the structure of the ANN model is determined. The network with the best prediction effect is then chosen. Figure 6 displays the regression diagram of the ANN model. With the testing set, the MSE value of the compressive strength prediction model is 1.662, and the MSE value of the fluidity prediction model is 2.327. Simultaneously, the fluidity prediction model has an *R*-value of 0.93, and the compressive strength prediction model has an *R*-value of 0.94, and both are extremely near to 1. There is a significant correlation between the model's predicted and experimental values, as evidenced by the *R*-values and MSE value of the ANN prediction model for compressive strength and workability, which illustrates the model's generalization capacity.

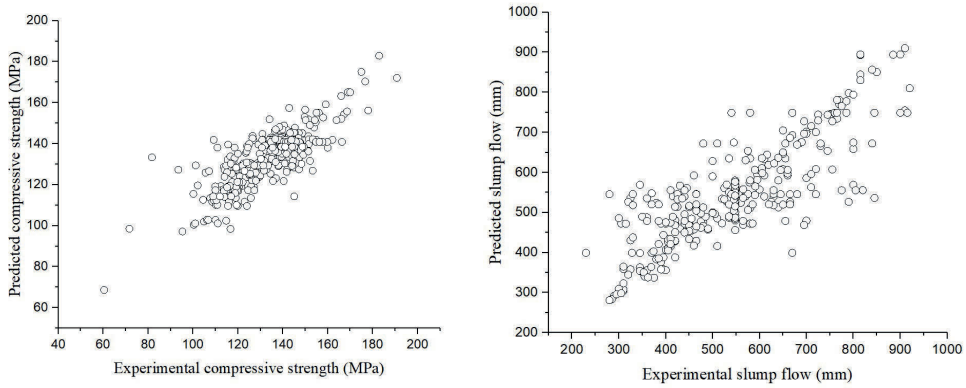

Figure 6. Regression diagram of the ANN model: (**a**) compressive strength (**b**) slump flow.

4.2.3. Comparison of ML Algorithms

To further examine the prediction ability of the ANN, XgBoost, extremely randomized tree, ridge, random forest, decision tree, gamma, AdaBoost, and gradient boosting are selected and implemented for comparison. The algorithm's *R* and *MSE* serve as the selection criteria. Table 4 shows the results of nine different ML techniques that are used to forecast the 28 d compressive strength and slump flow based on the dataset. The *R*-value of extremely randomized tree, ridge, random forest, decision tree, gamma, AdaBoost, and gradient boosting is less than 0.9, which presents a low prediction ability. Thus, out of the nine techniques, the ANN performs the best.

Table 4. The performance on datasets by 9 ML methods.

ML Method	Class	Dataset	MSE	R
XgBoost	Strength	Training	1.034	0.93
		Testing	3.213	0.89
	Slump flow	Training	1.3	0.92
		Testing	3.7	0.87
Extremely randomized tree	Strength	Training	0.31	0.92
		Testing	4.1	0.83
	Slump flow	Training	0.2	0.9
		Testing	2.1	0.878
Ridge	Strength	Training	5.104	0.904
		Testing	5.5	0.83
	Slump flow	Training	3.8	0.9
		Testing	5.2	0.88
Random Forest	Strength	Training	0.44	0.95
		Testing	2.77	0.91
	Slump flow	Training	2.2	0.91
		Testing	8.3	0.82
Decision Tree	Strength	Training	0.01	0.94
		Testing	5.4	0.91
	Slump flow	Training	1.9	0.89
		Testing	3.4	0.878
Gamma	Strength	Training	11.1	0.817
		Testing	11.9	0.79
	Slump flow	Training	9.1	0.83
		Testing	12.5	0.781
AdaBoost	Strength	Training	4.2	0.91
		Testing	5.5	0.84
	Slump flow	Training	3.1	0.9
		Testing	4.5	0.89
Gradient Boosting	Strength	Training	1.5	0.93
		Testing	5.5	0.88
	Slump flow	Training	3.2	0.89
		Testing	8.2	0.85
ANN	Strength	Training	0.412	0.95
		Testing	1.662	0.94
	Slump flow	Training	0.342	0.94
		Testing	2.327	0.93

4.2.4. Experimental Verification of ANN Model

For the validation experiment, 30 distinct mix proportions were designed. In accordance with the test procedure in Section 3, their slump flow and 28 d compressive strength are noted as test results. To acquire the prediction values, enter the mix ratio into the developed ANN prediction model. By comparing the errors between the experimental results and predicted values with the UHPC's compressive strength and slump flow, we can confirm the forecasting ability of the ANN model. The comparison outcomes are displayed in Figures 7 and 8.

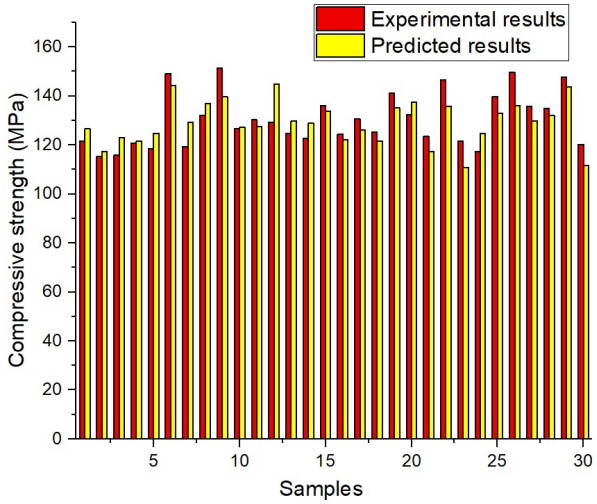

Figure 7. The predicted compressive strength of UHPC.

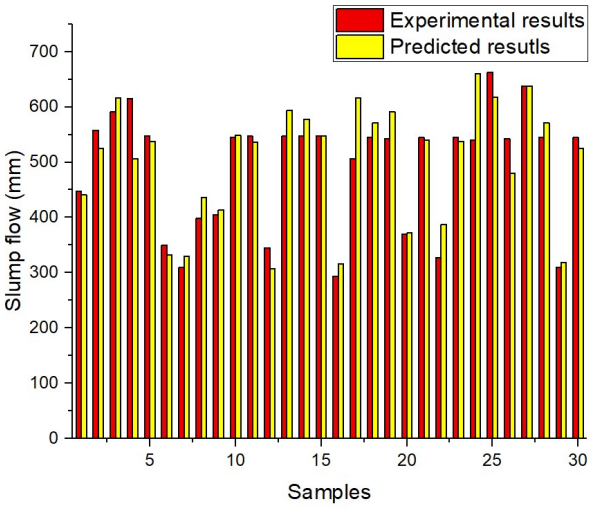

Figure 8. The predicted slump flow of UHPC.

The ANN-predicted values of 28 d compressive strength and slump flow corresponding to 30 groups of UHPC are within 10% of the experimental values. The accuracy of the ANN model's predictions is great. The findings show that the compressive strength and slump flow of UHPC can be reliably predicted by the ANN model. The prediction model's accuracy will increase as more data pertaining to UHPC are gathered. This further demonstrates that UHPC can be designed using ML models instead of requiring multiple UHPC trial mixes. The ANN model serves as the foundation for the GA optimization of the UHPC mix ratios.

4.3. GA Optimization Process

4.3.1. Optimization Objective Function

The eight parameters of cement content, fly ash content, GO content, silica fume content, fine aggregate content, water content, as well as the volume dosage of steel fibers, and the mass ratio of superplasticizer to cementitious materials in 1 m^3 UHPC were used as decision variables.

In optimization problems, the objective function is represented as a function of the decision variable, and the aim is to quantify the predicted outcome of the issue being optimized. The transportation between the equipment used in UHPC production and the raw materials is ignored here [56].

The goal of the UHPC mix ratio optimization is to minimize costs while still achieving the necessary levels of strength and workability. In essence, the previously developed prediction model for 28-day compressive strength and workability is a nonlinear functional connection between the UHPC's mix fraction and performance. Since the cost of UHPC is the study's optimization goal, we must also define the cost function as the optimization's objective function, as exhibited in Equation (4).

$$M_{COST} = C_C \cdot W_C + C_{Fl} \cdot W_{Fl} + C_{GO} \cdot W_{GO} + C_{Si} \cdot W_{Si} + C_{FA} \cdot W_{FA} + C_{SF} \cdot W_{SF} + C_{SP} \cdot W_{SP} + C_W \cdot W_W \quad (4)$$

Among them, C_C, C_{Fl}, C_{GO}, C_{Si}, C_{FA}, C_{SF}, C_{SP}, and C_W represent the unit mass cost of cement, fly ash, GO, silica fume, fine aggregate, steel fiber, superplasticizer, and water, respectively. W_C, W_{Fl}, W_{GO}, W_{Si}, W_{FA}, W_{SF}, W_{SP}, and W_W mean the mass of cement, fly ash, GO, silica fume, fine aggregate, steel fiber, superplasticizer, and water in 1 m^3 of UHPC, respectively. M_{COST} is the total cost of raw materials in 1 m^3 of UHPC.

The price information of UHPC's raw materials is exhibited in Table 5, and the price information comes from existing research [57–60]. Due to the input parameters of steel fiber in this study being the volume dosage, and superplasticizer being the ratio of its quality to the quality of cementitious materials, these two parameters are converted. According to the data in Table 5, the main reason for the high cost of UHPC is the high price of steel fibers, GO, and superplasticizers.

Table 5. Price of raw materials in UHPC.

Raw Material	Cost ($/ton)	References
Cement	82	[59]
Fly ash	40	[59]
GO	67,000	[60]
Silica fume	800	[59]
Fine aggregate	23.57	[58]
Steel fiber	5000	[59]
Superplasticizer	3400	[59]
Water	–	[57]

4.3.2. Constraint Condition

Constraints are mathematical functions of decision variables. In the GA method, the individual is infeasible and must be removed from the population when the constraints are not fulfilled. Thus, the constraints can act as independent functions of decision variables to place extra restrictions on the optimal solution, or they can act as constraints on both decision variables and objective functions. For example, the constraint on cement content is the limitation on decision variables in the field of optimization of the mix ratios. Meanwhile, the limitation on objective functions is the constraint on the slump flow and compressive strength. Compressive strength, workability, component content, component proportion, and absolute volume are the five constraint requirements that this study designs. The specific constraints are as follows.

1. Strength constraint. The 28-day compressive strength of UHPC should have a predicted value from the ANN that is higher than the required strength. Equation (5) illustrates the strength restriction.

$$f_c \geq f_{c,r} \quad (5)$$

Here, f_c is the predicted result of the 28-day compressive strength of UHPC, and $f_{c,r}$ is the required compressive strength in accordance with the real-world engineering requirements. Based on the fundamental mechanical characteristics of UHPC, $f_{c,r}$ is assumed in this study to be 120 MPa [61].

2. Slump flow constraint. The workability of fresh UHPC should be greater than the required workability. The workability constraint is displayed in Equation (6).

$$S \geq S_r \tag{6}$$

Among them, S is the predicted slump flow of fresh UHPC, and S_r is the required slump flow of fresh UHPC, which has to be chosen in accordance with the real engineering requirements. In this investigation, S_r is assumed to be 600 mm due to the fundamental working property of UHPC [62].

3. Component content constraint. This research employs the data range in the dataset as the component content constraint range, meaning that the optimized UHPC component content should fall within a suitable range. Table 6 displays the key statistical characteristics of the dataset, while Equation (7) shows the component content constraints.

$$W_l \leq W_{com} \leq W_u \tag{7}$$

Among them, W_{com} denotes the component content of each raw material, including cement, fly ash, GO, silica fume, fine aggregate, steel fiber, superplasticizer, and water. W_l and W_u are the lower and upper bounds for the component content.

Table 6. Statistical parameters of the component content in the dataset.

	Minimum Value	Maximum Value	Range
Cement (kg/m^3)	354	1000	646
Fly ash (kg/m^3)	0	328	328
GO (kg/m^3)	0	0.86	0.86
Silica fume (kg/m^3)	0	305	305
Fine aggregate (kg/m^3)	650	1718	1068
Steel fiber (vol.-%)	1.00	4.00	3.00
Superplasticizer (wt.%)	0.40	2.00	1.60
Water (kg/m^3)	142	241	99

4. Component proportion constraint. There are several related components in UHPC; hence, there should be limits on the ratios between these components. The ratios of cement to sand, water to cement, and water to binder have all been constrained in this investigation. As a component percentage limitation, we continue to use the dataset's proportion range. In Equations (8)–(10), the composition ratio constraints are illustrated. Table 7 lists the statistical parameters for the dataset's cement/sand, water/cement, and water/binder ratios.

$$R^l_{wc} \leq R_{wc} \leq R^u_{wc} \tag{8}$$

$$R^l_{wb} \leq R_{wb} \leq R^u_{wb} \tag{9}$$

$$R^l_{bfa} \leq R_{bfa} \leq R^u_{bfa} \tag{10}$$

where R_{wc}, R_{wb}, and R_{bfa} are the water/cement ratio, water/binder ratio, and cement/sand ratio, respectively. R^l and R^u are the lower and upper bounds of the composition proportion.

Table 7. Statistical parameters of the component proportion in the dataset.

	Minimum Value	Maximum Value	Average Value
R_{wc}	0.140	0.477	0.239
R_{wb}	0.120	0.300	0.171
R_{bfa}	0.68	1.43	1.03

5. Absolute volume constraint. The volume of UHPC should be equal to the sum of the volumes of all components. The absolute volume constraint is illustrated in Equation (11).

$$\frac{W_C}{\rho_C} + \frac{W_{Fl}}{\rho_{Fl}} + \frac{W_{Si}}{\rho_{Fl}} + \frac{W_{FA}}{\rho_{FA}} + \frac{W_{SF}}{\rho_{SF}} + \frac{W_{SP}}{\rho_{SP}} + \frac{W_W}{\rho_W} = 1 \quad (11)$$

where ρ_C, ρ_{Fl}, ρ_{Si}, ρ_{FA}, ρ_{SF}, ρ_{SP}, and ρ_W are the densities of cement, fly ash, silica fume, fine aggregate, steel fiber, superplasticizer, and water, respectively. Table 1 lists the densities of the cementitious materials. Meanwhile, the densities of fine aggregate, steel fiber, superplasticizer, and water are 2630 kg/m^3, 7800 kg/m^3, 1190 kg/m^3, and 1000 kg/m^3, respectively.

4.3.3. Cost Optimization of UHPC

The GA can be used to optimize the UHPC mix ratio once the optimization objective function and constraint conditions have been established. The UHPC mix ratio serves as the basis for both the optimization objective function and the five constraint conditions. Through the GA, it consistently lowers the cost of UHPC while maintaining a performance that can satisfy real-world engineering requirements.

By modifying the hyperparameters, this study sets the population size (*NP* = 453), maximum iteration count (*maxgen* = 200), crossover probability (*Pc* = 0.9), and mutation probability (*Pm* = 0.1) in the GA [12]. The iteration curve of the GA is depicted in Figure 9. During the iteration process, the UHPC cost function continuously decreases through initialization, fitness calculation, selection operation, crossover operation, and mutation operation, ultimately obtaining the optimal mix ratio of UHPC. Figure 9 shows that the value of the optimization objective function, or more specifically, the UHPC cost function, keeps decreasing as the population keeps iterating. The cost function value is found to essentially stay constant until the number of iterations approaches 160, suggesting that the GA has attained the convergence threshold and that a maximum of 200 iterations is appropriate for this investigation.

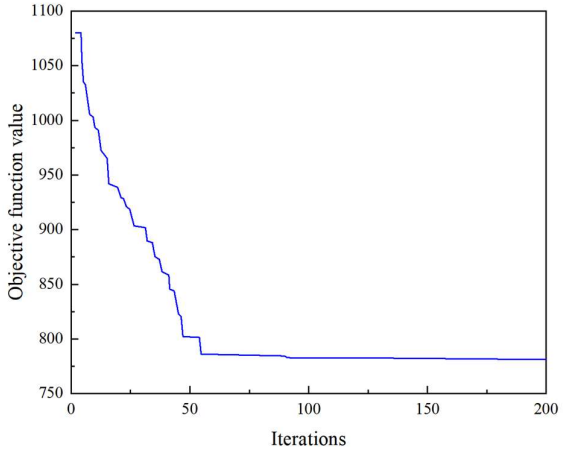

Figure 9. Optimization of UHPC cost using GA.

4.4. Optimization Results and Experimental Verification

UHPC costs are becoming cheaper in the iterative GA process. Ultimately, one set of UHPC mix proportions that satisfy the specified constraint constraints and have the lowest cost are identified. Table 8 presents the optimal mix ratio. The predicted slump flow is 603 mm, the predicted 28 d compressive strength is 120 MPa, and the genetic algorithm-optimized cost is 776 \$/m^3. In North America, the cost of a 1 m^3 of UHPC for engineering purposes is currently between 1000 and 2620 \$/m^3 [59]. The cost associated with the genetic algorithm-optimized UHPC mix proportion has dropped dramatically.

Table 8. Mix ratio for UHPC with the lowest cost.

Cement (kg)	Fly Ash (kg)	GO (kg)	Silica Fume (kg)	Fine Aggregate (kg)	Steel Fiber (vol.%)	Superplasticizer (wt%)	Water (kg)
675.1	185.7	0.300	137.3	950.6	1.36	1.36	190.4

UHPC specimens are formed in the laboratory according to the optimized, low-cost mix ratio and subjected to work performance and mechanical tests. After the experiment, the 28 d compressive strength is 121.5 MPa, with a slump flow of 620 mm. The discrepancy between the experimental compressive strength and the predicted value is 1.2%, while the error between the experimental slump flow and the predicted result is 2.8%. Further, the constraints are satisfied.

By improving the microstructures of UHPC and boosting compressive, tensile, and flexural strengths, GO can raise the overall performance of UHPC. By using GO, it can be found from Table 8 that expensive components such as steel fibers, water-reducing agents, and silica fume are decreased since GO can increase the mechanical properties of UHPC. On the other hand, GO is used in UPHC at extremely low contents. This is so the costs are lowered due to the usage of GO.

5. Sensitivity Analysis

To encourage the engineering use of UHPC, it is crucial to do factor sensitivity analysis. Sensitivity analysis on input parameters is conducted by calculating the MIV and evaluating the impact of each input parameter in the UHPC mix ratio on the 28 d compressive strength and slump flow of UHPC. The calculation of the MIV value is based on the developed ANN model. The input parameters of cement, fly ash, GO, silica fume, fine aggregate, steel fiber, superplasticizer, and water are defined as X1–X8, with a 20% threshold as the lower limit for selecting important variables [63]. The calculation results of the MIV values are shown in Figures 10 and 11. The symbol represents the positive and negative correlations in which the input parameter is related to the output parameter. If the MIV is positive, the input parameter is positively related to the output parameter. If the MIV is negative, then the input parameter is negatively related to the output parameter. The absolute value denotes the relative importance of the influence.

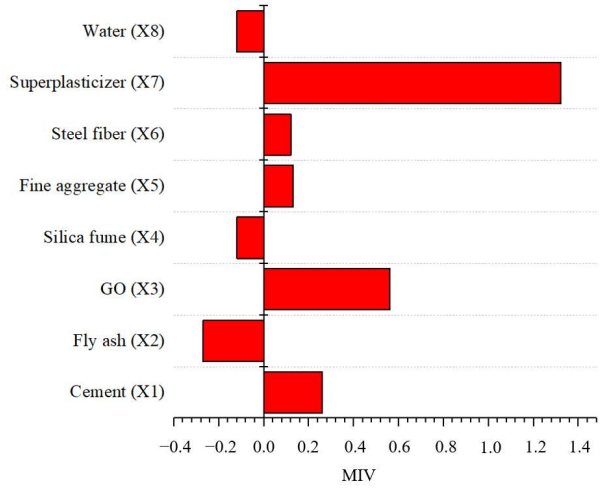

Figure 10. MIV of 28 d compressive strength.

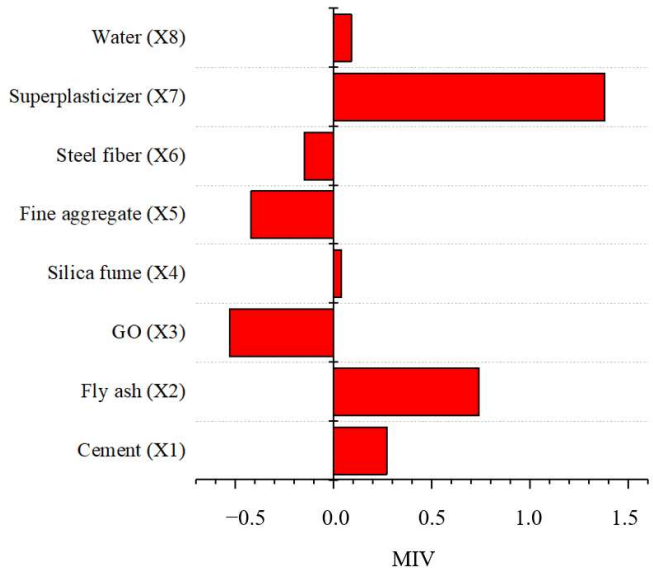

Figure 11. MIV of slump flow.

According to Figure 10, the cement content, fly ash content, GO content, and superplasticizer content have a strong correlation with the compressive strength of UHPC and can be regarded as important variables. From the positive and negative values of each parameter MIV, it can be seen that the cement content, GO content, and superplasticizer content are positively correlated with the 28-day compressive strength of UHPC, while the fly ash content is negatively correlated with the 28-day compressive strength of UHPC.

As the cement dosage increases, the water/cement ratio decreases. When the water/cement ratio of UHPC is too high, it will also generate a large number of pores during the hydration process, reducing the compactness of UHPC. Therefore, the compressive strength of UHPC decreases with the increase of the water/cement ratio [64], and the cement content is positively correlated with the compressive strength of UHPC. Fly ash has pozzolanic activity, with the main components being SiO_2 and Al_2O_3. It can react with free $Ca(OH)_2$ to form hydrates with cementitious properties. The UHPC that contains fly ash has a lower 28-day compressive strength due to a low speed of secondary hydration [65]. Therefore, the amount of fly ash added is negatively correlated with the compressive strength of UHPC. The superplasticizer has a great impact on the packing density of UHPC, and the optimized amount of superplasticizer can significantly increase the packing density of UHPC [66]. Therefore, the amount of superplasticizer is positively correlated with the compressive strength of UHPC. According to our own previous experiments, GO promotes the cement hydration process, reduces the most probable pore diameter of the matrix, reduces porosity, and makes the matrix denser [32]. The two-dimensional planar structure of GO prevents and delays the development of cracks, leading to crack deflection and changing the path of crack development. After the cracks encounter GO, some cracks are blocked and no longer expand. Some cracks develop along the GO towards both ends, significantly increasing the path of crack development, maximizing the dispersion of stress energy, and improving the bearing capacity. The mechanism of GO enhancing UHPC is to effectively prevent and delay the propagation of microcracks through the filling effect, deflection effect, bridging effect, and pull-out effect [67]. In addition, the nanoscale matrix-reinforcement effect provided by GO will further have a positive impact on the pull-out performance of steel fibers. GO and steel fibers exhibit good synergistic crack control effects [46]. The addition of GO can significantly increase the energy dissipated through friction at the fiber–matrix interface. Hence, the amount of GO is positively correlated with the compressive strength of UHPC.

From Figure 11, the cement content, fly ash content, GO content, fine aggregate content, and superplasticizer content have a strong correlation with the fluidity of UHPC and can be

regarded as important variables. From the positive and negative values of each parameter MIV, it can be seen that the cement content, fly ash content, GO content, and superplasticizer content are positively correlated with UHPC's fluidity, while the fine aggregate content is negatively correlated with UHPC's fluidity.

When the water consumption is constant, the greater sand/cement ratio leads to the larger particles and internal pores in UHPC increase, leading to an increase in water in the pores and a decrease in particle surface water. It results in a decrease in UHPC fluidity. Therefore, the cement content is positively correlated with UHPC workability, while the fine aggregate dosage is negatively correlated with UHPC's fluidity. Fly ash has a spherical structure and smooth surface. In the early stage of UHPC hydration, it can play a flocculent role, reducing water consumption and improving the fluidity of fresh UHPC. Polycarboxylic acid water-reducing agents have carboxyl side chains and polyoxyethylene side chains, which can, respectively, improve the dispersion and plastic retention properties of UHPC and correspondingly increase its flowability. With an increased GO content, the fluidity of UHPC shows a decreasing trend. This is because GO has a larger specific surface area, which allows its surface to absorb more free water and water-reducing agents, resulting in a decrease in the fluidity of UHPC [68].

Although the cost of industrial-grade graphene oxide is still high, its usage in UHPC is small, and it can significantly improve the compressive strength of UHPC. When its content is lower than 0.05%, GO has a small influence on the flowability of UHPC [68]. Hence, GO has great potential for use in UHPC.

6. Conclusions

This study developed a nonlinear functional relationship between the properties of UHPC and its mix ratio in order to optimize the mix ratio of UHPC using ML techniques. Based on this, the cost of UHPC is optimized, and the optimal mix ratio is obtained using the GA. The work significantly contributes to the application of GO-modified UHPC in engineering.

First, a dataset with the 28 d compressive strengths and slump flows for eight raw materials for UHPC was developed. Next, employing ANN, a prediction model for UHPC compressive strength and workability was developed. Further, the performance of nine distinct ML methods was compared. The ANN model has a maximum prediction accuracy when the number of hidden layer neurons is 16, according to the evaluation indicators such as *R* and *MSE*. Based on the ANN model, the GA was used to optimize the UHPC cost functions. Significantly less than the average cost of UHPC, at 776 $\$/m^3$, is the cost corresponding to the optimal low-cost UHPC mix ratio. Finally, the MIV was used to evaluate the importance of the input parameters of UHPC on its compressive strength and fluidity. The four input parameters of cement content, fly ash content, GO content, and superplasticizer content have a significant impact on the compressive strength and fluidity of UHPC. Based on the experimental and theoretical research, the main cost of GO-modified UHPC comes from steel fibers and silica fume, and GO has the potential to be used in UHPC to reduce its cost and improve its properties.

Author Contributions: Conceptualization, S.Z.; methodology, M.D.; validation, M.D.; investigation, M.D. and Z.L.; writing—original draft preparation, H.L. and M.D.; writing—review and editing, S.Z.; visualization, H.L.; supervision, S.Z.; project administration, L.X.; funding acquisition, L.X. All authors have read and agreed to the published version of the manuscript.

Funding: This research was funded by the National Key R&D Program of China (Grant No. 2022YFB2602600) and the National Natural Science Foundation of China (No. 52002040).

Data Availability Statement: The original contributions presented in this study are included in the article. Further inquiries can be directed to the corresponding author.

Conflicts of Interest: Authors Hui Lv and Li Xiao were employed by the company China Merchants Chongqing Communications Technology Research and Design Institute Co., Ltd. The remaining

authors declare that the research was conducted in the absence of any commercial or financial relationships that could be construed as potential conflicts of interest.

References

1. Amran, M.; Huang, S.S.; Onaizi, A.M.; Makul, N.; Abdelgader, H.S.; Ozbakkaloglu, T. Recent trends in ultra-high performance concrete (UHPC): Current status, challenges, and future prospects. *Constr. Build. Mater.* **2022**, *352*, 129029. [CrossRef]
2. Zeyad, A.M.; Hakeem, I.Y.; Amin, M.; Tayeh, B.A.; Agwa, I.S. Effect of aggregate and fibre types on ultra-high-performance concrete designed for radiation shielding. *J. Build. Eng.* **2022**, *58*, 104960. [CrossRef]
3. Yoo, D.Y.; Oh, T.; Banthia, N. Nanomaterials in ultra-high-performance concrete (UHPC)—A review. *Cem. Concr. Compos.* **2022**, *134*, 104730. [CrossRef]
4. Zasypkina, A.; Ivanova, N.; Spasov, D.; Mensharapov, R.; Alekseeva, O.; Vorobyeva, E.; Kukueva, E.; Fateev, V. Electrode with a carbon nanotube array for a proton exchange membrane fuel cell. *Inorganics* **2023**, *11*, 219. [CrossRef]
5. Alshahrie, A.; Alghamdi, A.; Hasan, P.; Ahmed, F.; Albalawi, H.; Umar, A.; Alsulami, A. Enhancement in the performance of dye sensitized solar cells (DSSCs) by incorporation of reduced graphene oxide (RGO) and carbon nanotubes (CNTs) in ZnO nanostructures. *Inorganics* **2023**, *10*, 204. [CrossRef]
6. Chu, H.Y.; Jiang, J.Y.; Sun, W.; Zhang, M.Z. Mechanical and thermal properties of graphene sulfonate nanosheet reinforced sacrificial concrete at elevated temperatures. *Constr. Build. Mater.* **2017**, *153*, 682–694. [CrossRef]
7. Newell, M.; Garcia-Taengua, E. Fresh and hardened state properties of hybrid graphene oxide/nanosilica cement composites. *Constr. Build. Mater.* **2019**, *221*, 433–442. [CrossRef]
8. Wu, Y.Y.; Zhang, J.; Liu, C.J.; Zheng, Z.L.; Lambert, P. Effect of graphene oxide nanosheets on physical properties of ultra-high-performance concrete with high volume supplementary cementitious materials. *Materials* **2020**, *13*, 1929. [CrossRef]
9. Alatawna, A.; Birenboim, M.; Nadiv, R.; Buzaglo, M.; Peretz-Damari, S.; Peled, A.; Regev, O.; Sripada, R. The effect of compatibility and dimensionality of carbon nanofillers on cement composites. *Constr. Build. Mater.* **2020**, *232*, 117141. [CrossRef]
10. Chu, H.Y.; Zhang, Y.; Wang, F.J.; Feng, T.T.; Wang, L.G.; Wang, D.N. Effect of graphene oxide on mechanical properties and durability of ultra-high-performance concrete prepared from recycled sand. *Nanomaterials* **2020**, *10*, 1718. [CrossRef]
11. Luo, Q.Z.; Wu, Y.Y.; Qiu, W.J.; Huang, H.L.; Pei, S.F.; Lambert, P.; Hui, D. Improving flexural strength of UHPC with sustainably synthesized graphene oxide. *Nanotechnol. Rev.* **2021**, *10*, 754–767. [CrossRef]
12. Wang, M.; Du, M.F.; Jia, Y.; Chang, C.; Zhou, S. Carbon emission optimization of ultra-high-performance concrete using machine learning methods. *Materials* **2024**, *17*, 1670. [CrossRef]
13. Zhou, S.; Li, Z.J.; Li, K.; Jia, Y.; Wang, C.; Zhuang, X.Y. Microcapsule-enabled self-healing concrete: A bibliometric analysis. *Front. Struct. Civ. Eng.* **2023**, *17*, 1611–1629. [CrossRef]
14. Zhu, H.L.; Wu, X.; Luo, Y.L.; Jia, Y.; Wang, C.; Fang, Z.; Zhuang, X.Y.; Zhou, S. Prediction of early compressive strength of ultrahigh-performance concrete using machine learning methods. *Int. J. Comput. Methods* **2023**, *20*, 2141023. [CrossRef]
15. Zhou, S.; Jia, Y.; Wang, C. Global sensitivity analysis for the polymeric microcapsules in self-healing cementitious composites. *Polymers* **2020**, *12*, 2990. [CrossRef]
16. Sun, J.B.; Ma, Y.Z.; Li, J.X.; Zhang, J.F.; Ren, Z.H.; Wang, X.Y. Machine learning-aided design and prediction of cementitious composites containing graphite and slag powder. *J. Build. Eng.* **2021**, *43*, 102544. [CrossRef]
17. Sun, J.B.; Wang, X.Y.; Zhang, J.F.; Xiao, F.; Sun, Y.T.; Ren, Z.H.; Zhang, G.B.; Liu, S.K.; Wang, Y.F. Multi-objective optimisation of a graphite-slag conductive composite applying a BAS-SVR based model. *J. Build. Eng.* **2021**, *44*, 103223. [CrossRef]
18. Feng, W.H.; Wang, Y.F.; Sun, J.B.; Tang, Y.C.; Wu, D.X.; Jiang, Z.W.; Wang, J.Q.; Wang, X.Y. Prediction of thermo-mechanical properties of rubber-modified recycled aggregate concrete. *Constr. Build. Mater.* **2022**, *318*, 125970. [CrossRef]
19. Zhang, J.F.; Sun, Y.T.; Li, G.C.; Wang, Y.H.; Sun, J.B.; Li, J.X. Machine-learning-assisted shear strength prediction of reinforced concrete beams with and without stirrups. *Eng. Comput.* **2022**, *38*, 1293–1307. [CrossRef]
20. Sun, J.B.; Wang, J.Q.; Zhu, Z.Y.; He, R.; Peng, C.; Zhang, C.; Huang, J.Z.; Wang, Y.F.; Wang, X.Y. Mechanical performance prediction for sustainable high-strength concrete using bio-inspired neural network. *Buildings* **2022**, *12*, 65. [CrossRef]
21. Sun, J.B.; Wang, Y.F.; Liu, S.K.; Dehghani, A.; Xiang, X.L.; Wei, J.J.; Wang, X.Y. Mechanical, chemical and hydrothermal activation for waste glass reinforced cement. *Constr. Build. Mater.* **2021**, *301*, 124361. [CrossRef]
22. Farooq, F.; Amin, M.N.; Khan, K.; Sadiq, M.R.; Javed, M.F.; Aslam, F.; Alyousef, R. A comparative study of random forest and genetic engineering programming for the prediction of compressive strength of high strength concrete (HSC). *Appl. Sci.* **2020**, *10*, 7330. [CrossRef]
23. Al-Shamiri, A.K.; Kim, J.H.; Yuan, T.F.; Yoon, Y.S. Modeling the compressive strength of high-strength concrete: An extreme learning approach. *Constr. Build. Mater.* **2019**, *208*, 204–219. [CrossRef]
24. Lee, J.H.; Yoon, Y.S.; Kim, J.H. A new heuristic algorithm for mix design of high-performance concrete. *KSCE J. Civ. Eng.* **2012**, *16*, 974–979. [CrossRef]
25. Cheng, M.Y.; Prayogo, D.; Wu, Y.W. Novel genetic algorithm-based evolutionary support vector machine for optimizing high-performance concrete mixture. *J. Comput. Civ. Eng.* **2014**, *28*, 06014003. [CrossRef]
26. Hinton, G.E.; Williams, R.J. Learning representations by back-propagating errors. *Nature* **1986**, *323*, 533–536.
27. Holland, J.H. *Adaptation in Natural and Artificial Systems: An Introductory Analysis with Applications to Biology, Control, and Artificial Intelligence*; University of Michigan Press: Ann Arbor, MI, USA, 1975.

28. Türkeli, E.; Öztürk, H.T. Optimum design of partially prestressed concrete beams using Genetic Algorithms. *Struct. Eng. Mech.* **2017**, *64*, 579–589.
29. Stone, M. Cross-validatory choice and assessment of statistical predictions. *J. R. Stat. Soc. Ser. B-Stat. Methodol.* **1974**, *36*, 111–147. [CrossRef]
30. *GB/T31387-2015*; Reactive Power Concrete. Chinese National Standards: Beijing, China, 2015. (In Chinese)
31. Wang, M.; Yao, H. Comparison study on the adsorption behavior of chemically functionalized graphene oxide and graphene oxide on cement. *Materials* **2020**, *13*, 3274. [CrossRef]
32. Xiong, G.; Ren, Y.; Wang, C.; Zhang, Z.; Zhou, S.; Kuang, C.; Zhao, Y.; Guo, B.; Hong, S. Effect of power ultrasound assisted mixing on graphene oxide in cement paste: Dispersion, microstructure and mechanical properties. *J. Build. Eng.* **2023**, *69*, 106321. [CrossRef]
33. Luo, Y.; Yu, Z.P. Effect of graphene oxide on mechanical properties of UHPC and analysis of micro-control mechanism. *Mater. Res. Express* **2021**, *8*, 095001.
34. Xiong, G.Q.; Ren, Y.L.; Jia, X.L.; Fang, Z.; Sun, K.K.; Huang, Q.; Wang, C.; Zhou, S. Understanding the influence of ultrasonic power on the hydration of cement paste. *J. Build. Eng.* **2024**, *87*, 108996. [CrossRef]
35. Xiong, G.; Wang, C.; Zhou, S.; Zhao, Y.; Li, Y.; Liu, Y.; Qiu, J. Effect of power ultrasound-assisted mixing on the hydration and microstructural development of cement paste, *J. Sustain. Cem. Based* **2023**, *12*, 1061–1072. [CrossRef]
36. Xiong, G.Q.; Wang, C.; Zhou, S.; Zheng, Y.L.; Ren, Y.L.; Fang, Z.; Zhao, Y. Understanding the thermal effect of power ultrasound in cement paste. *Appl. Therm. Eng.* **2023**, *232*, 120946. [CrossRef]
37. *GB/T2419-2005*; Test Method for Fluidity of Cement Mortar. Chinese National Standards: Beijing, China, 2005. (In Chinese)
38. Esmaeili, J.; Romouzi, V.; Kasaei, J.; Andalibi, K. An investigation of durability and the mechanical properties of ultra-high performance concrete (UHPC) modified with economical graphene oxide nano-sheets. *J. Build. Eng.* **2023**, *80*, 107908. [CrossRef]
39. Yang, K.; Long, G.C.; Tang, Z.; Wu, H.; Ma, G.; Cheng, Z.Q.; Xiang, Y.; Xie, Y.J. Enhancement in strength and toughness of ultra-high performance concrete (UHPC) from micron- and nano-scale. *J. Build. Eng.* **2023**, *69*, 106308. [CrossRef]
40. Luo, Y.K.; Yu, Z.P. Effects of graphene oxide on durability of ultra high performance concrete. *Funct. Mater.* **2022**, *29*, 135–143.
41. Yu, L.Z.; Wu, R.X. Using graphene oxide to improve the properties of ultra-high-performance concrete with fine recycled aggregate. *Constr. Build. Mater.* **2020**, *259*, 120657. [CrossRef]
42. Paredes, J.A.; Gálvez, J.C.; Enfedaque, A.; Alberti, M.G. Matrix optimization of Ultra High Performance Concrete for improving strength and durability. *Materials* **2021**, *14*, 6944. [CrossRef] [PubMed]
43. Regalla, S.; Kumar, N.S. Influence of graphene oxide in the hydration mechanism by reinforcing mechanical strength and microstructural characterization of ultra-high-performance concrete (UHPC). *J. Dispers. Sci. Technol.* **2023**, *1*, 1–18. [CrossRef]
44. Chu, H.Y.; Qin, J.J.; Gao, L.; Jiang, J.Y.; Wang, F.J.; Wang, D.Q. Effects of graphene oxide on mechanical properties and microstructure of ultra-high-performance lightweight concrete. *J. Sustain. Cem. Based Mater.* **2023**, *12*, 647–660. [CrossRef]
45. Cheng, S.K.; Chen, K.; Wu, Q.Y.; Chen, X.Y.; Zhao, C.; Wu, Z.Y. Influence of industrial-grade graphene oxide on macro and micro properties of ultra-high performance concrete incorporating recycled fine aggregate. *Constr. Build. Mater.* **2024**, *417*, 135427. [CrossRef]
46. Yu, L.B.; Bai, S.; Guan, X.C. Effect of multi-scale reinforcement on fracture property of ultra-high performance concrete. *Constr. Build. Mater.* **2023**, *397*, 132383. [CrossRef]
47. Mao, K.H.; Yu, J.M.; Yang, B.; Liu, H.X.; Shen, L.; Elchalakani, M.; Alqawzai, S. Mechanical properties of graphene oxide modified ultra-high-performance concrete containing coarse aggregate. *J. Build. Eng.* **2024**, *86*, 108754. [CrossRef]
48. Lamastra, F.R.; Bavasso, I.; Bracciale, M.P.; Duranti, L.; Montesperelli, G.; Di Palma, L.; Bianco, A. Toward clima-resilient ultra-high performance concrete (UHPC): A survey on high-strength mortars engineered with extra-low dosage graphene-based materials (GBMs). *Ceram. Int.* **2023**, *49*, 38482–38498. [CrossRef]
49. Deeb, R.; Karihaloo, B.L. Mix proportioning of self-compacting normal and high-strength concretes. *Mag. Concr. Res.* **2013**, *65*, 1200164. [CrossRef]
50. Ayira, F.; John, O. Investigating the Properties of Reactive Powder Concrete (RPC)—Compressive and Flexural Strength. Ph.D. Thesis, Universiti Teknologi Petronas, Bandar Seri Iskandar, Malaysia, 2013.
51. Amin, M.; Zeyad, A.M.; Tayeh, B.A.; Agwa, I.S. Effect of ferrosilicon and silica fume on mechanical, durability, and microstructure characteristics of ultra high-performance concrete. *Constr. Build. Mater.* **2022**, *320*, 126233. [CrossRef]
52. Nie, J.; Li, C.; Qian, G.; Pan, R.; Fei, B.; Deng, S. Effect of shape and content of steel fiber on workability and mechanical properties of Ultra-High Performance Concrete (UHPC). *Cailiao Daobao/Mater. Rep.* **2021**, *35*, 04042–04052.
53. Pyo, S.; Kim, H.K. Fresh and hardened properties of ultra-high performance concrete incorporating coal bottom ash and slag powder. *Constr. Build. Mater.* **2017**, *131*, 459–466. [CrossRef]
54. Randl, N.; Steiner, T.; Ofner, S.; Baumgartner, E.; Mészöly, T. Development of UHPC mixtures from an ecological point of view. *Constr. Build. Mater.* **2014**, *67*, 373–378. [CrossRef]
55. Ghafari, E.; Bandarabadi, M.; Costa, H.; Júlio, E. Prediction of fresh and hardened state properties of UHPC: Comparative study of statistical mixture design and an artificial neural network model. *J. Mater. Civ. Eng.* **2015**, *27*, 04015017. [CrossRef]
56. Kim, T.; Tae, S.; Roh, S. Assessment of the CO_2 emission and cost reduction performance of a low-carbon-emission concrete mix design using an optimal mix design system. *Renew. Sust. Energ. Rev.* **2013**, *25*, 729–741. [CrossRef]

57. Wille, K.; Boisvert-Cotulio, C. Material efficiency in the design of ultra-high performance concrete. *Constr. Build. Mater.* **2015**, *86*, 33–43. [CrossRef]
58. Shi, J.Y.; Tan, J.X.; Liu, B.J.; Chen, J.Z.; Dai, J.D.; He, Z.H. Experimental study on full-volume slag alkali-activated mortars: Air-cooled blast furnace slag versus machine-made sand as fine aggregates. *J. Hazard Mater.* **2021**, *403*, 123983. [CrossRef] [PubMed]
59. Alsalman, A.; Dang, C.N.; Martí-Vargas, J.R.; Hale, W.M. Mixture-proportioning of economical UHPC mixtures. *J. Build. Eng.* **2020**, *27*, 100970. [CrossRef]
60. Tucker, J.L. Laboratory Evaluation, Mechanistic Performance Prediction, and Life Cycle Cost Analysis (LCCA) of Graphene Oxide Modified Asphalt Binders. Master's Thesis, University of Colorado at Boulder, Boulder, CO, USA, 2023.
61. Roberti, F.; Cesari, V.F.; de Matos, P.R.; Pelisser, F.; Pilar, R. High- and ultra-high-performance concrete produced with sulfate-resisting cement and steel microfiber: Autogenous shrinkage, fresh-state, mechanical properties and microstructure characterization. *Constr. Build. Mater.* **2021**, *268*, 121092. [CrossRef]
62. Shin, T.Y.; Kim, J.H.; Koh, K.T.; Ryu, G.S.; Wang, K.J. Placement of ultra-high performance concrete for inclined-surface pavement. *Road Mater. Pavement Des.* **2022**, *23*, 1667–1680. [CrossRef]
63. Abuodeh, O.R.; Abdalla, J.A.; Hawileh, R.A. Assessment of compressive strength of Ultra-high Performance Concrete using deep machine learning techniques. *Appl. Soft Comput.* **2020**, *95*, 106552. [CrossRef]
64. Chen, Y.; Liu, P.; Sha, F.; Yin, J.; He, S.S.; Li, Q.H.; Yu, Z.W.; Chen, H.L. Study on the mechanical and rheological properties of ultra-high performance concrete. *J. Mater. Res. Technol-JMRT* **2022**, *17*, 111–124. [CrossRef]
65. Yu, R.; Spiesz, P.; Brouwers, H.J.H. Development of an eco-friendly Ultra-High Performance Concrete (UHPC) with efficient cement and mineral admixtures uses. *Cem. Concr. Compos.* **2015**, *55*, 383–394. [CrossRef]
66. Wang, X.P.; Yu, R.; Song, Q.L.; Shui, Z.H.; Liu, Z.; Wu, S.; Hou, D.S. Optimized design of ultra-high performance concrete (UHPC) with a high wet packing density. *Cem. Concr. Res.* **2019**, *126*, 105921. [CrossRef]
67. Cui, K.; Chang, J. Hydration, reinforcing mechanism, and macro performance of multi-layer graphene-modified cement composites. *J. Build. Eng.* **2022**, *57*, 104880. [CrossRef]
68. Meng, W.N.; Khayat, K.H. Mechanical properties of ultra-high-performance concrete enhanced with graphite nanoplatelets and carbon nanofibers. *Compos. Part B Eng.* **2016**, *107*, 113–122. [CrossRef]